

## Physical investigations on Cu/ Bi<sub>2</sub>O<sub>3</sub> structure for potential applications

K. Ben Bacha\*<sup>1</sup>, T. Larbi<sup>1</sup>, J. Bennaceur<sup>2</sup>, M. Amlouk<sup>1</sup>

Corresponding author, E-mail: benbachakawther@gmail.com

1 : Nanomaterials, Nanotechnology and Energy Laboratory (LNNE), physics department, Faculty of Sciences of Tunis, Tunis El Manar University, Tunisia.

2 : Energy Research and Technology Center, Potovoltaic Laboratory (LPV).

### Abstract

Undoped Bismuth trioxides (Bi<sub>2</sub>O<sub>3</sub>) thin films were prepared using the spray pyrolysis technique at 350°C on glass substrates. Cu/ Bi<sub>2</sub>O<sub>3</sub> structures were obtained when deposited by means of the thermal evaporation of 10 nm of Cu metal onto Bi<sub>2</sub>O<sub>3</sub> sprayed thin films and then treated at 500°C using a thermal programmable oven during 1h. First, obtained thin films of Cu doped Bi<sub>2</sub>O<sub>3</sub> as well as undoped ones were characterized using X-ray diffraction (XRD), Raman spectroscopy, ultraviolet–visible absorbance spectroscopy (UV–vis) and the impedance spectroscopy. According to X-ray diffraction results undoped samples have two peaks related to cubic phase of Bismuth trioxide (Bi<sub>2</sub>O<sub>3</sub>) while the doped ones crystallize in the same phase with a Copper oxide (CuO) as minority phase. Second, the band gap energy value decreases from 3.96 to 3.87 eV with Cu doping. The impedance measurements indicate firstly that the conductivity increases with the increasing of both the temperature and the frequency. On the other hand, calculated values of the activation energy increase in terms of Cu doping. Also, the electrical conductivity is thermally activated well as the relaxation times distribution. Finally, these doped films may be of interest for various applications as bio and gas sensors.

**Keywords:** Bismuth trioxide, Cu doping, thin film, spray, the band gap energy, conductivity,...

Date of Submission: 15-05-2022

Date of Acceptance: 30-05-2022

### I. Introduction

The large-scale industrialization and rapid population augmentation are increasing the rate of fossil fuel consumption, leading to a severe environmental pollution that has a detrimental cause on living beings. Remediation of these environmental pollutants in water as well as in air by photo-catalytic process has attracted great interest in recent two decades [1-3]. Many studies have focused on the efficiency of energy use to meet the increasing demand for energy. The sun is a primary source of energy and the use of its energy is of critical importance.

Among different photocatalysts such as titanium dioxide (TiO<sub>2</sub>), zinc oxide (ZnO), zirconium oxide (ZrO<sub>2</sub>), cadmium sulfide (CdS), tungsten trioxide (WO<sub>3</sub>) and zinc sulfide (ZnS), TiO<sub>2</sub>, due to its low cost, abundance, non-toxicity, high oxidation power and high resistance to photocorrosion, has been widely tested in water purification systems [4].

However, bismuth-based semiconductors are receiving increased attention as photocatalysts that degrade organic pollutants under UV-vis light [5-12]. In particular, bismuth oxide (Bi<sub>2</sub>O<sub>3</sub>) [13-15] has various desirable properties including high band gap (2-3.96 eV), high refractive index and photoluminescence. This oxide is used in many fields such as solid oxide fuel cells, gas sensors, high temperature superconducting materials, functional ceramics, and catalysis [6,7].

It is worth noting to point out that Bi<sub>2</sub>O<sub>3</sub> is non-toxic and has high refractive index, dielectric permittivity, and ionic and photonic conductivity, suggesting a candidate anode material for photo-induced water splitting [16, 17]. The nanostructuring may reduce optical losses by improving reflection and optical losses [18]. In addition, pillars composed of nanoparticles can significantly improve light absorption [18, 19].

Bismuth trioxide, Bi<sub>2</sub>O<sub>3</sub>, is widely used in industry, especially in solid electrolytes and fuel cells. Recently, due to its wide band gap, semiconducting behavior, high ionic conductivity, high refractive index, gas sensitivity, notable photoconductivity and photoluminescence, Bi<sub>2</sub>O<sub>3</sub> is gaining more attention. These physical properties are making bismuth trioxide a candidate for applications in the domains of electronic circuits, coating optics, UV radiation detection, photovoltaics and gas sensors [20, 21].

The spray pyrolysis technique has been used for thin films coating because it is a simple and cost-effective process that leads to uniform film growth [22,24-25] as compared to other chemical techniques such as dip coating, CVD or MOCVD [30,23,26,27].

In parallel to the investigation of different substrates, emphasis was also placed on the use of visible light for photocatalytic evaluation of the films. Tetragonal beta-bismuth oxide ( $\beta$ -Bi<sub>2</sub>O<sub>3</sub>) was chosen as the immobilized photocatalyst because it is a very promising material for visible light [22, 28, 29]. On the other hand, The investigation confirms that the novel ternary Bi<sub>2</sub>O<sub>3</sub>-CuO-CuBi<sub>2</sub>O<sub>4</sub> photocatalysts synthesized by the solvothermal show wide application prospect in wastewater remediation [31]. So, new research is found to indicate that a 2D ultrathin Cu- $\delta$ -Bi<sub>2</sub>O<sub>3</sub> nanosheets possess excellent photocatalytic nitrogen fixation without any sacrificial agent [32].

It is widely used in applications, such as microelectronics, and sensor and optical technology [33].

The use of bismuth oxide (Bi<sub>2</sub>O<sub>3</sub>) in industry is quite broad as it is an important semiconductor with excellent optical and electrical properties such as high refractive index, high dielectric strength and good photoconductivity. Bismuth oxide is found in six different polymorphic structures. Its most important applications are therefore the manufacture of high quality optical fibers, doped bismuth oxide fibers, photoelectric materials, transparent ceramic glass, oxide varistors, electrical sensors and high temperature doped superconductors [34].

## II. Experimental section

### 2.1 Deposition of Bi<sub>2</sub>O<sub>3</sub> films

The precursor solution for the Bi<sub>2</sub>O<sub>3</sub> films was prepared by mixing 1.08 g of bismuth(III) nitrate pentahydrate (Bi(NO<sub>3</sub>)<sub>3</sub>·5H<sub>2</sub>O,  $\geq 98\%$ , Sigma-Aldrich) in 10 mL acetic acid (CH<sub>3</sub>COOH, 99.7%, Samchun Chemicals) at 25 °C (room temperature, RT) with stirring at 500 rpm for 30 min. The complete dissolution of Bi(NO<sub>3</sub>)<sub>3</sub> in CH<sub>3</sub>COOH produced a transparent solution. The precursor solution was then deposited on a pre-cleaned glass substrate measuring 1.5 × 1.5 cm<sup>2</sup>, by the spray process. This solution flow rate is approximately 4 ml/ min through a 0.5-mm-diameter nozzle. The nozzle-to-substrate distance was equal to 30 cm and the substrate temperature was maintained at 350 °C. The spraying time of 30 was chosen. The as deposited Bi<sub>2</sub>O<sub>3</sub> was white in color.

For the preparation of the Cu/Bi<sub>2</sub>O<sub>3</sub> structure, a high-purity Cu (Aldrich, 99.9%) was deposited by thermal evaporation. The copper metallic was placed on a furnace-fired tantalum filament, evacuated to a pressure of  $4.8 \times 10^{-6}$  mbar, and a current was applied to the crucibles for 1 min to evaporate the 110 variac solid ( $I = 150$  A). After depositing 10 nm of copper on the Bi<sub>2</sub>O<sub>3</sub> surface, the Cu/ Bi<sub>2</sub>O<sub>3</sub> bilayers were annealed during 60 min in air at a temperature of 500 °C in a programmable oven. Indeed, during this annealing process, the copper migrated inside Bi<sub>2</sub>O<sub>3</sub> layer giving rise to a Cu doped film.

### 2.2 Experimental Techniques

The structural properties were reached using a Philips X'PertX-ray diffractometer with CuK $\alpha$  radiation with  $\lambda = 1.5405980$  Å (40 kV, 30 mA). Optical transmittance and reflectance were measured at room temperature and at normal incidence with UV-vis-NIR Shimadzu 3100S spectrophotometer in the wavelength range of 300–1800 nm. Raman spectra recorded between 100 cm<sup>-1</sup> and 4000 cm<sup>-1</sup> of as prepared thin films were measured in the backscattering configuration using a Labram single monochromator Raman spectrometer at excitation wavelength  $\lambda = 632.8$  nm with a charge coupled device detector allowing a resolution of 1 cm<sup>-1</sup>.

The electrical measurements of real and imaginary components of impedance parameters ( $Z'$  and  $Z''$ ) were made over a wide range of temperature (350–490 °C) and frequency (1 Hz–13 MHz) by means of a Hewlett-Packard HP 4192 impedance analyzer.

## III. Results and interpretations

### 3.1 Structural properties

**Fig. 1a** shows patterns of the undoped and Cu-doped Bi<sub>2</sub>O<sub>3</sub> sprayed thin films. As can be seen in **Fig. 1a**, the diffractions peaks at 31.30° and 66.13° indexed with (002) and (004) are the characteristic planes of the fluorite-type cubic structure with space group (Fm3m). The sharp peak in XRD pattern indicates the high degree of crystallinity of undoped Bi<sub>2</sub>O<sub>3</sub>. We note that after copper doping, the intensity of (002) peak decreases (**Fig. 1b**). It is worthy noted that the low intensity diffraction peak positioned at 11.84° corresponding to the CuO, clearly proves that Cu doping to achieve a phase change in the bismuth oxide of Bi<sub>2</sub>O<sub>3</sub>. This trend was known as Vergard's law which stated that the lattice parameters depended on the composition [35].

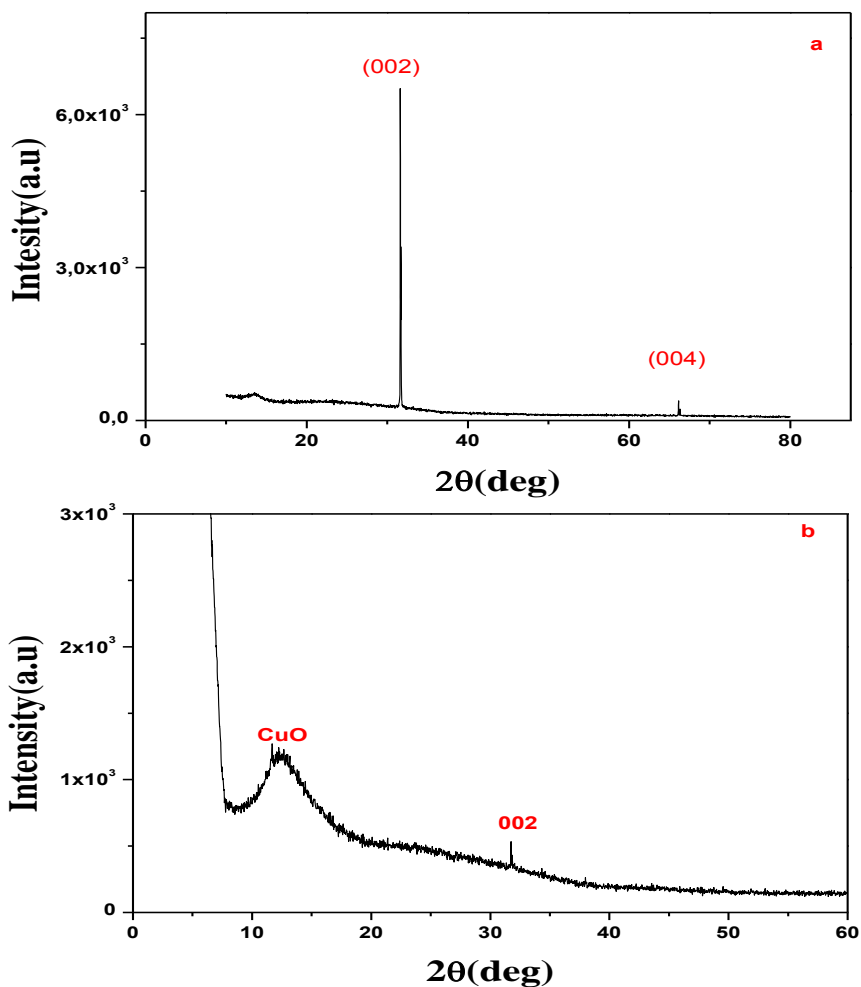


Fig. 1: X-ray diffractograms of a) Bi<sub>2</sub>O<sub>3</sub>, b) Cu: Bi<sub>2</sub>O<sub>3</sub> sprayed at 350°C.

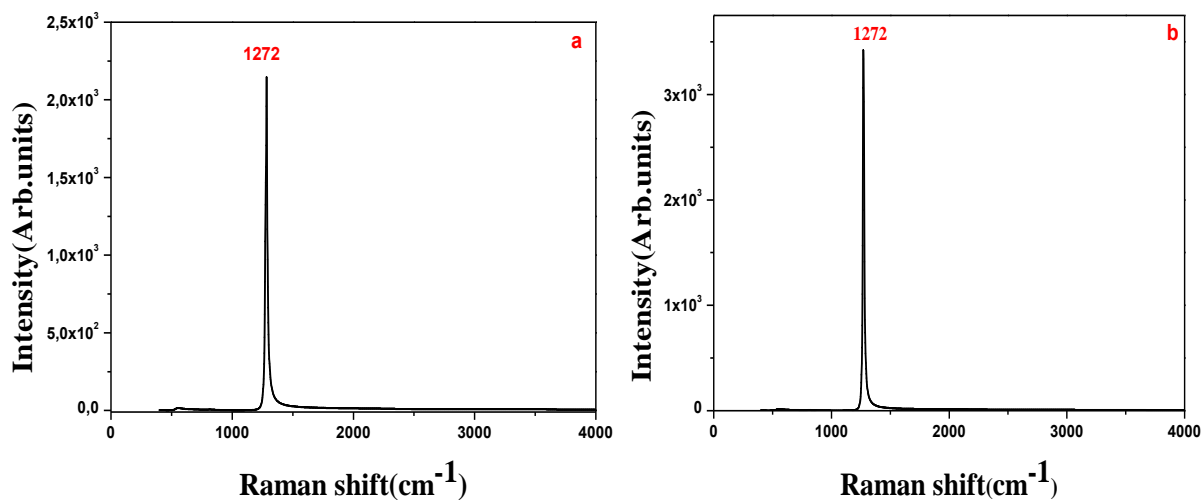
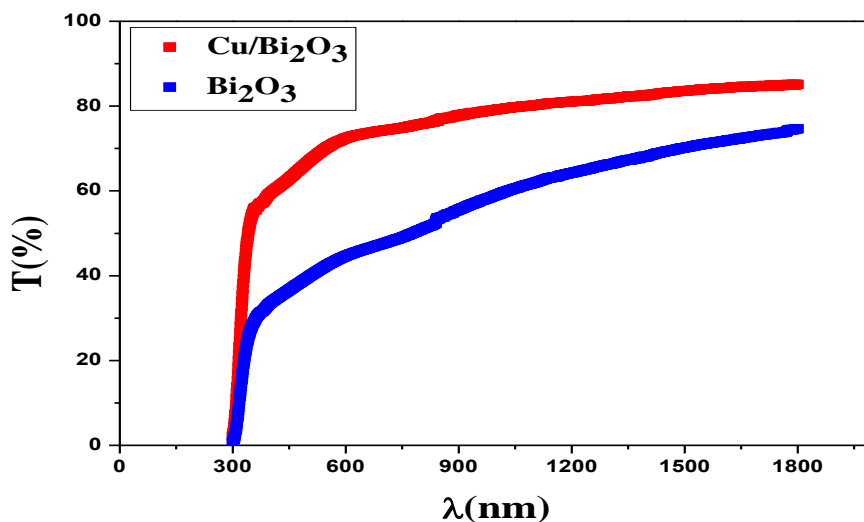


Fig.2: Spectrum of Raman of a) Bi<sub>2</sub>O<sub>3</sub> and b) Cu: Bi<sub>2</sub>O<sub>3</sub> sprayed at 350°C.

On the other hand, several details on the microstructure and crystallographic defects are provided by Raman spectroscopy. Indeed, **Fig. 2** depicts Raman spectra of undoped and Cu-doped Bi<sub>2</sub>O<sub>3</sub> thin films. At a first glance, we can see an intense peak located at 1272 cm<sup>-1</sup> at the two spectrum corresponds to Bi–O vibration, the only difference is the intensity of this peak as reported by Feng He et al [36].

### 3.2 Optical properties

UV-visible spectroscopy was used to characterize the optical transmittance and reflexion of undoped and Cu-doped Bi<sub>2</sub>O<sub>3</sub> thin films in the wavelength region of 300–1800 nm. The spectra are shown in **Fig.3**. All films are a thickness of the order of 100 nm. It can be seen that the interference fringe patterns are absent in all transmittance spectra due to weak multiple reflections at the interface. These two films show a relatively high transparency. Indeed, the transmission in visible region is found to be minimum for undoped Bi<sub>2</sub>O<sub>3</sub> film (50 %) and increased with Cu content to reach 75 %.



**Fig. 3:** Spectrum of Transmittance of Bi<sub>2</sub>O<sub>3</sub> and Cu: Bi<sub>2</sub>O<sub>3</sub> sprayed at 350°C.

The UV–vis absorption spectra of the prepared thin films as well as band gap energy measurements are shown in **Fig.4 and 5**, respectively. The absorbance edges of the prepared samples were located approximately at the wavelength range from 400 to 500 nm.

In order to determine the optical band gap for such glasses, the absorption coefficient ( $\alpha$ ) below and near the fundamental absorption edge can be calculated from the formula [37]:

$$\alpha = \frac{1}{d} \ln \left( \frac{(1-R)^2}{T} \right) \quad \text{Eq.1}$$

Here T is the transmittance; R is the reflectance and d is the film thickness ( $d = 1 \mu\text{m}$ ).

The absorption edge of Cu-doped Bi<sub>2</sub>O<sub>3</sub> films to a larger wavelength. This phenomenon indicates that the optical energy gap decreases with doping, which it was determined using this formula:

$$(\alpha h\nu) = A(h\nu - E_g)^{1/2} \quad \text{Eq.2}$$

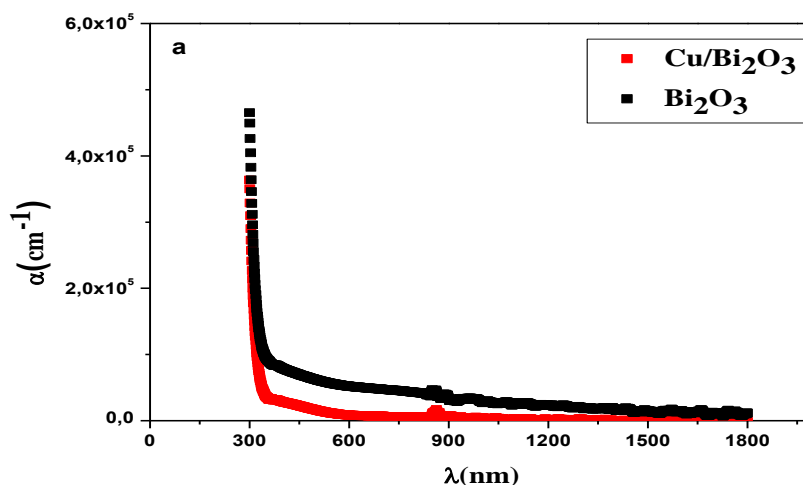


**Fig.4:** Spectrums of  $\alpha$  ( $\text{cm}^{-1}$ ) of Bi<sub>2</sub>O<sub>3</sub> and Cu: Bi<sub>2</sub>O<sub>3</sub> sprayed at 350°C.

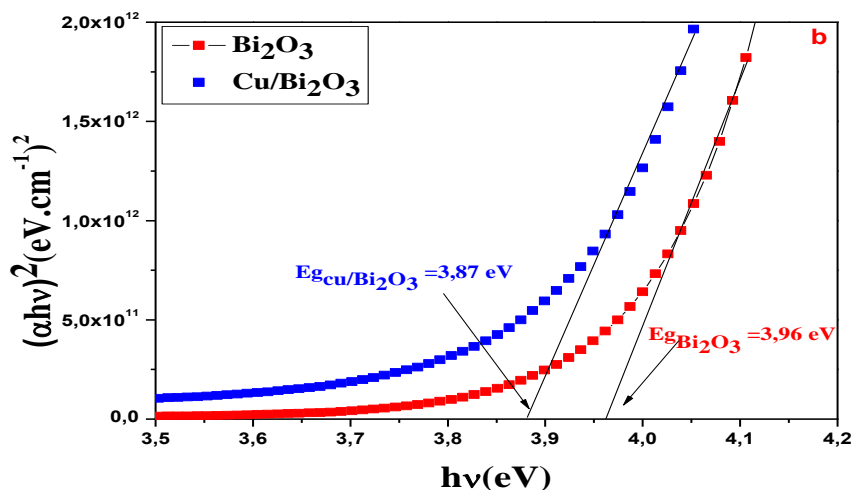


**Fig.5: Spectrums of  $(\alpha h\nu)^2 (eV \cdot cm^{-1})^2$  of Bi<sub>2</sub>O<sub>3</sub> and Cu: Bi<sub>2</sub>O<sub>3</sub> sprayed at 350°C.**

All the samples showed an improvement in the photo absorbance properties in the visible region up to 1800 nm, as shown in **Fig. 4**. The sharpness of the absorption edges indicated the good crystalline nature of the prepared samples [38].

The band gap energies ( $E_g$  values) of the samples could thus be estimated from the plot of  $(\alpha h\nu)^2$  versus photon energy ( $h\nu$ ) for the direct transition or the plot of  $(\alpha h\nu)^{1/2}$  versus photon energy ( $h\nu$ ) for the indirect transition. Both band gap values of as-prepared Bi<sub>2</sub>O<sub>3</sub> and Cu: Bi<sub>2</sub>O<sub>3</sub> films were 3.96 and 3.87 eV, respectively (**Fig. 5**). It is found that these band gap values are significantly similar to the result obtained by Z. Hamid and T. R. Das et al. such as a wide energy gap change (from 2 to 3.96 eV) [39,40]. But, it is higher than the KLE-templated films can readily produce phase-pure  $\beta$ -Bi<sub>2</sub>O<sub>3</sub> with an optical band gap of about 3.4 eV obtained by Brezesinski et al. [41]. Thus, in other research the band gaps for Bi/Bi<sub>2</sub>O<sub>3</sub> and rGO@Bi/Bi<sub>2</sub>O<sub>3</sub> were 3.5 and 3 eV, respectively obtained by Merfat Algethami [42]. While, K. B. Kusuma et al. Found an energy bandgap ( $E_g$ ) value of 3.3 eV [43].

These variations in band gap energy values depended on the preparation technologies, preparation conditions, micro-structure and particle size of the prepared thin films. It was clear that there was an improvement following Cu<sup>2+</sup> doping in the Bi<sub>2</sub>O<sub>3</sub> crystal lattice, leading to a decrease in particle size, and modification of the energy gap as previously reported [44].

It is known that the narrower band gap of Bi<sub>2</sub>O<sub>3</sub> permits absorbance of more visible light to generate charge carriers. As-deposited film without doping is white in color, but is transformed to beige with doping by copper. This change is due to the transformation in the composition of Bi<sub>2</sub>O<sub>3</sub> and it seems consistent with previous works [45].

### 3.3 Electrical properties

The electrical responses thin films were studied using the complex impedance technique in a wide frequency range from 100 Hz to 13 MHz and at temperatures between 350°C and 490 °C. The curves ( $Z''$  vs  $Z'$ ) extracted from the impedance spectroscopy measurements is given in **Fig. 6**.

Fig.6a shows that the Bi<sub>2</sub>O<sub>3</sub> thin film exhibits two compressed semicircles that depict data taken at different temperatures in all compositions that exhibit both grain effects (bulk property) and grain boundary effects. The contribution positioned at a low frequency corresponds to the grain boundary response; at the high frequency, it corresponds to the specific bulk property. All the semicircles depict a degree of depression instead of a real  $Z''$  axis which is centred on the semicircle that may be due to a relaxation time distribution. The depression of the semicircle is considered to further pressure evidence for polarization phenomena along with a relaxation time distribution (non-Debye type relaxation). Such non-ideal behavior can be assigned to several factors such as grain orientation, grains boundaries, stress-strain phenomena as well as atomic defect distribution.

But this attitude disappears in Bi<sub>2</sub>O<sub>3</sub> doped with Cu (**Fig.6b**). Indeed, these traces are composed of a semicircle moved with respect to the origin and are not focused on the real axis. Their radius reduces with increasing temperature because of the several types of dipoles present in the material. These observations allow us to conclude that the electrical conductivity is activated thermally as well as the distribution of the relaxation times.

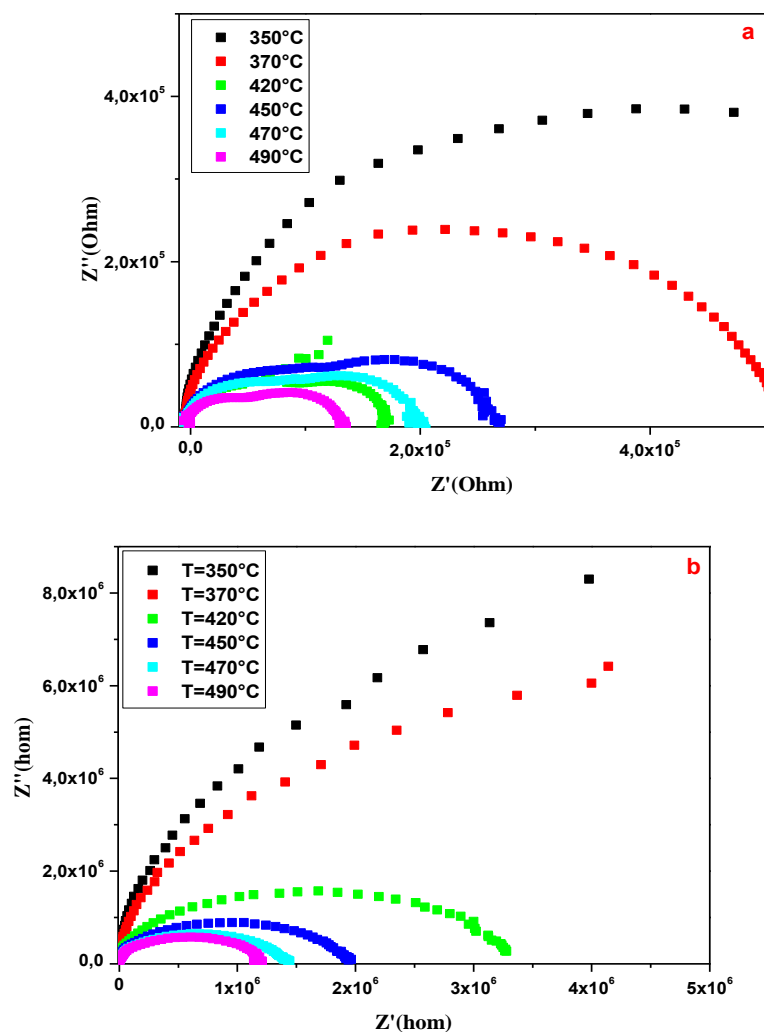


**Fig.6: Complex impedance spectra at different temperatures of a) Bi<sub>2</sub>O<sub>3</sub> and b) Cu: Bi<sub>2</sub>O<sub>3</sub> sprayed at 350°C.**

In order to study the relaxation time as a function of temperature, we plot  $Z''$  versus frequency at different. Indeed, **Fig.7** shows the plot of the imaginary part  $Z''$  as a function of frequency at different temperatures that increase monotonously with increasing frequency. These curves are characterized by a maximum peak at a particular frequency. It is known that  $Z''$  passes through a maximum at  $\omega_m \tau = 1$ . This peak has a tendency to move towards high frequencies with an asymmetrical expansion suggesting the existence of a distributed relaxation process [46].

This phenomenon reveals that the peak frequency indicating Arrhenius behavior and then we can determine the activation energy. The relaxation time  $\tau$  of these samples obeys to the well-known Arrhenius law (**Eq. 3**) [47]:

$$\omega_m = \omega_0 e^{-\frac{E_a}{k_b T}} \quad \text{Eq.3}$$

where  $E_a$  is the activation energy, and  $\omega_0$  is a distinctive frequency.

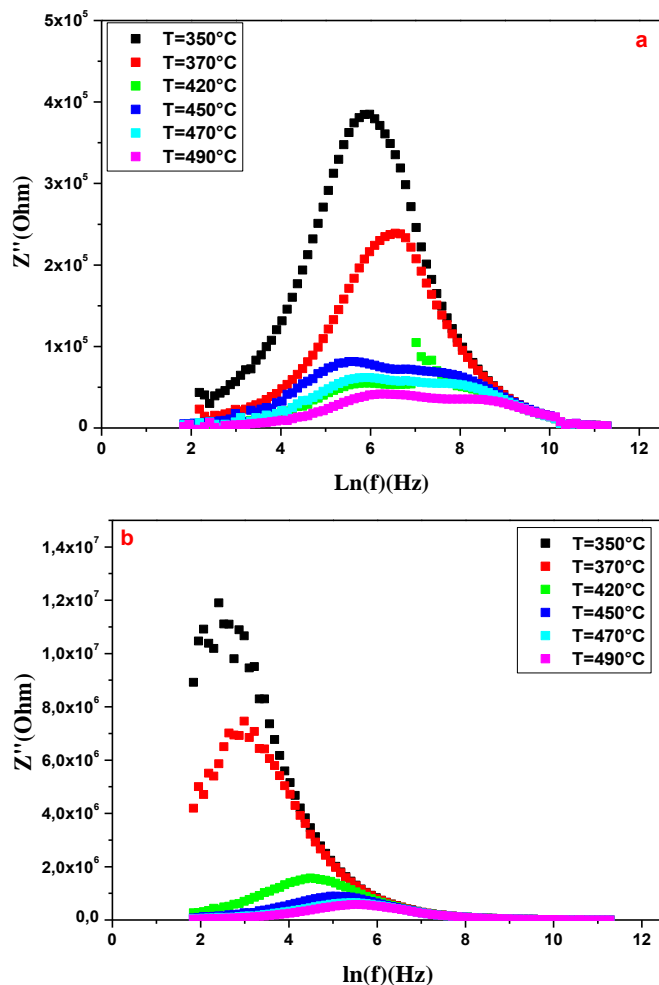


Fig.7: Angular frequency dependence of  $Z''$  of a)  $\text{Bi}_2\text{O}_3$  and b) Cu:  $\text{Bi}_2\text{O}_3$  sprayed at 350°C.

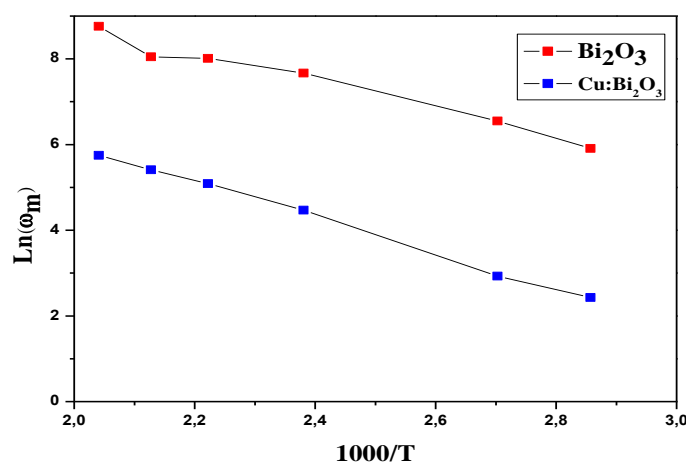


Fig.8: spectrum of  $\ln(\omega_m)$  versus  $f(1000/T)$  of  $\text{Bi}_2\text{O}_3$  and b) Cu:  $\text{Bi}_2\text{O}_3$  sprayed at 350°C.

The fit of the  $\ln(\omega_m)$  vs  $(1000/T)$  (as seen in Fig. 8) leads to the calculation of the activation energies  $E_a$  (eV) which are recapitulated in Table 1. The calculated values of the activation energy increase after doping. Also the thin film undoped  $\text{Bi}_2\text{O}_3$  has two activation energies following the depression of the semicircle and the existence of grain and grain boundaries.

**Table.1:** Calculated values of E<sub>a</sub> of a) Bi<sub>2</sub>O<sub>3</sub> and b) Cu: Bi<sub>2</sub>O<sub>3</sub> sprayed at 350°C.

	Activation Energy (E <sub>a</sub> ) (10 <sup>-4</sup> eV)	
	E <sub>a</sub> <sup>1</sup>	E <sub>a</sub> <sup>2</sup>
Bi <sub>2</sub> O <sub>3</sub>	1.599	2.743
Cu : Bi <sub>2</sub> O <sub>3</sub>	-	3.586

The global conductivity of the films can be governed by Jonscher’s law of universal power [47]:

$$\sigma_t = \sigma_{DC} + \sigma_{AC} \tag{Eq.4}$$

where is the dc conductivity, which is calculated by extrapolating the curves of  $\sigma_t$  at zero frequency for different temperatures. In the higher frequency range, the conductivity increases linearly with increasing frequency.

**Fig. 9** stands for the typical plot of  $\ln(\sigma_t)$  as a function of  $\ln(\omega)$  at different temperatures for both undoped and doped Cu Bi<sub>2</sub>O<sub>3</sub> films. In the high-frequency range, the conductivity increases linearly in terms of the frequency for all samples. On the contrary, at low frequencies, the conductivity is almost independent of frequency, which could be attributed to the DC contribution.

As the conductivity increases with the rise of the temperature, the AC conductivity turns to a higher frequency with the temperature. This is consistent with the shift in relaxation frequency. From the result regarding the jump frequency and DC conductivity, it can be assumed that the conduction path is related to a similar transport mechanism.

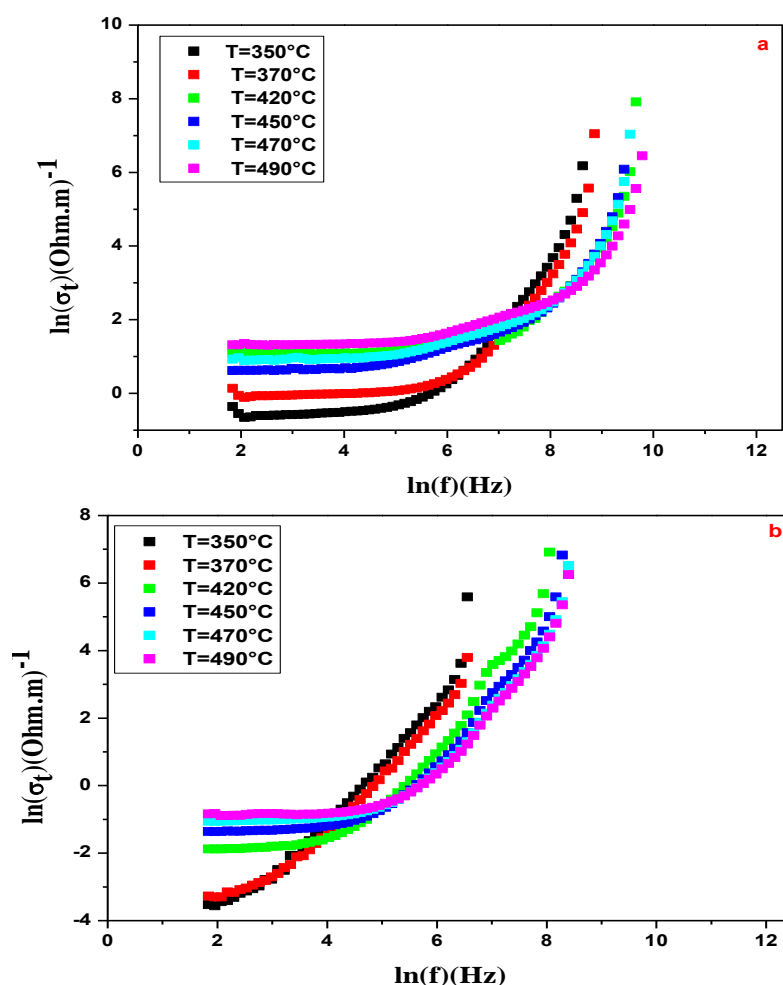


**Fig.9:** Angular frequency dependence of AC conductivity at different temperature of a) Bi<sub>2</sub>O<sub>3</sub> and b) Cu: Bi<sub>2</sub>O<sub>3</sub> sprayed at 350°C.

#### IV. Conclusion:

This work addresses the protocol of the preparation of Cu-doped Bi<sub>2</sub>O<sub>3</sub> thin films by both methods such as the spray pyrolysis and the thermal evaporation. Various techniques are used to analyze their physical properties. The XRD study indicates a cubic phase with the crystallites oriented in the (002) direction. Further, the addition of copper leads to the emergence of the secondary phase of CuO. Cu-doped layers exhibited an average optical transmittance of 75% in the visible range. It was observed that obtained Cu/Bi<sub>2</sub>O<sub>3</sub> structure may be used in photocatalysis. On the other hand, the study of the mechanism of electrical conduction inside that in the high frequency range, the conductivity increases linearly with frequency for all samples, while at low frequencies it is almost independent with frequency, which might be ascribed to the contribution of direct current that it makes Bi<sub>2</sub>O<sub>3</sub> a good conductor to be used in the manufacture of various devices such as electrical sensors and high temperature doped superconductors. Further studies are in progress to test these doped films as gas sensors, as photocatalysts and so on.

#### References:

- [1]. M.R. Hoffmann, S.T. Martin, W. Choi, D.W. Bahnemann, Chem. Rev. 95, 69 (1995).
- [2]. A. Kubacka, M. Fernandez-Garcia, G. Colon, Chem. Rev. 112, 1555 (2012).
- [3]. A.L. Linsebigler, G. Lu, J.T. Yates, Chem. Rev. 95,735(1995).
- [4]. S.O.-B. Oppong, F. Opoku, P.P. Govender, Appl. Catal. B 243,106–120 (2019).
- [5]. J. Cao, X. Li, H. Lin, S. Chen, X. Fu, J. Hazard. Mater.,316, 239–240 (2012).
- [6]. C. Pan, X. Li, F. Wang, L. Wang, Ceram. Int. 34, 439(2008).
- [7]. W. Xiaohong, Q. Wei, H. Weidong, J. Mol.Catal. A: Chem. 261, 167 (2007).
- [8]. H. Weidong, Q. Wei, W. Xiaohong, N. Hailong, Mater. Lett. 61, 4100 (2007).
- [9]. B. Sirota, J. Reyes-Cuellar, P. Kohli, L. Wang, M.E. McCarroll,S.M. Aouadi, Thin Solid Films 520,6113 (2012).
- [10]. S. Shenawi-Khalila, V. Uvarovb, E. Menesa, I. Popovb, Y.Sassona, Appl. Catal. A: Gen., 1, 413–414 (2012).
- [11]. T.-D. Nguyen-Phan, V.H. Pham, E.W. Shin, H.-D. Pham, S. Kim,J.S. Chung, E.J. Kim, S.H. Hur, Chem. Eng. J. 170 , 226 (2011).
- [12]. H. Lachheb, E. Puzenat, A. Houas, M. Ksibi, E. Elaloui, C. Guil-lard, J.-M. Herrmann, Appl. Catal.B: Environ. 39, 75(2002).
- [13]. L. Zhou, W. Wang, H. Xu, S. Sun, M. Shang, Chem. Eur. J. 15, 1776 (2009).
- [14]. H. Cheng, B. Huang, J. Lu, Z. Wang, B. Xu, X. Qin, X. Zhang, Y.Dai, Phys. Chem. Chem. Phys. 12,15468 (2010).
- [15]. L. Zhang, W. Wang, J. Yang, Z. Chen, W. Zhang, L. Zhou, S. Liu, Appl. Catal. A: Gen. 308, 105(2006).
- [16]. K.S. Al-Namshah, R.M. Mohamed, Applied Nanoscience. 1-7 (2018).
- [17]. Y. Bao, T.-T. Lim, Z. Zhong, R. Wang, X. Hu, J. Colloid Interface Sci. 505, 488-499 (2017).
- [18]. M.L. Brongersma, Y. Cui, S. Fan, Nat. Mater. 13, 451 (2014).
- [19]. M.-W. Kim, K. Kim, T.Y. Ohm, H. Yoon, B. Joshi, E. Samuel, M.T. Swihart, S.K. Choi, H. Park, S.S. Yoon, Chem. Eng. J. 333, 721-729 (2018).
- [20]. S. Condurache-Bota, in: Y. Zhou Ed. Bismuth-Advanced Applications and Defects Characterization, (IntechOpen Limited, London, United Kingdom, 2018), p. 171–204.
- [21]. S.S. Bhande, R.S. Mane, A.V. Ghule, S.-H. Han, Scr. Mater. 65, 1081–1084 (2011).
- [22]. K. Barrera-Mota, M. Bizarro, M. Castellino, A. Tagliaferro, A. Hernández, S.E. Rodil, Photochem. Photobiol. Sci. 14, 1110–1119 (2015).
- [23]. S.J. Moniz, C.S. Blackman, C.J. Carmalt, G. Hyett, J. Mater. Chem. 20,7881–7886(2010).
- [24]. M. Bizarro, E. Martínez-Padilla, Thin Solid Films. 553, 179–183 (2014).
- [25]. Nora S. Portillo-Vélez, M. Bizarro, J. Nanomater. 2016, 1-11 (2016).
- [26]. C.M. Ling, A.R. Mohamed, S. Bhatia, Chemosphere. 57, 547–554 (2004).
- [27]. Z. Ding, X. Hu, G.Q. Lu, P.-L. Yue, P.F. Greenfield, Langmuir. 16, 6216–6222 (2000).
- [28]. X. Xiao, R. Hu, C. Liu, C. Xing, C. Qian, X. Zuo, J. Nan, L. Wang, Appl. Catal. B Environ. 140, (2013) 433–443.
- [29]. Y. Lu, Y. Zhao, J. Zhao, Y. Song, Z. Huang, F. Gao, N. Li, Y. Li, Cryst. Growth Des. 15, 1031–1042 (2015).
- [30]. X. Zhang, M. Zhou, L. Lei, Carbon. 44, 325–333(2006).
- [31]. Junwei Hou Yu Xie, Yarong Sun, Yu Kuang, Zhihao Jiao, Qingyao Wang, Ceramics International, Available online 11 April 2022.
- [32]. Xiaoming Gao, Kaixuan Xu, Hongbing He, Shouda Liu, Xiangbo Zhao, Available online 2 April 2022.
- [33]. Lili Ding, Qian Zhao, Jingli Zhu, Zengjie Fan, Bin Liu, International Conference on Materials Chemistry and Environmental Protection (MEEP 2015).
- [34]. A. Elizarraras-Peñalosa, M. Estrada-Flores, C.M. Reza-San Germán, M.E. Manríquez Ramírez, Superficies y Vacío 32 (2019) 14-21.
- [35]. M. Saraiva, V. Georgieva, S. Mahieu, K.V. Aeken, A. Bogaerts, D. Depla, J. Appl. Phys. 107, 1–10 (2010).
- [36]. Feng He, Zijun He, Junlin Xie, Yuhui Li, American Journal of Analytical Chemistry. 5, 1142-1150 (2014).
- [37]. T.B. Nasr, N. Kamoun, M. Kanzari, R. Bennaceur, Thin Solid Films. 500, 4–8 (2006)
- [38]. N. Mukherjee, B. Sho, S.K. Maji, U. Madhu, S.K. Bhar, B.C. Mitra, G.G. Khan, A. Mondal, Mater. Lett. 65, 3248–3250 (2011).
- [39]. Z. Hamid, Australian journal of basic and applied sciences, vol. 7, pp. 97–101, 2017.
- [40]. T. R. Das, S. Patra, R. Madhuri, and K. P. Sharma, Journal of colloid and interface science, vol. 509, pp. 82–93, 2018.
- [41]. K. Brezesinski, R. Ostermann, P. Hartmann, J. Perlich, T. Brezesinski, Chem. Mater. 22, 3079–3085 (2010).
- [42]. Merfat Algethami, Mater. Res. Express 9 (2022) 025001.
- [43]. K. B. Kusuma , M. Manju , C. R. Ravikumar , V. G. Dileepkumar , A. Naveen Kumar , Mysore Sridhar Santosh , H. C. Ananda Murthy and K. Gurushantha, Hindawi Journal of Nanomaterials,13 (2022)1-13.
- [44]. L. Li, P.A. Salvador, G.S. Röhrer, Nanoscale. 6, 24–42(2014).
- [45]. Sh. Labib, Journal of Saudi Chemical Society. 21, 664-672 (2017).
- [46]. T. Nagata, T. Shimura, A. Ashida, N. Fujimura, T. Ito, J Crystal Growth . 237, 533–537 (2002).
- [47]. N. Kilinc, S. Ozturk, L. Arda, A. Altındal, Z.Z. Ozturk, J. Alloys Compd. 536, 138–144 (2012).